9th International Food Operations & Processing Simulation Workshop
20th International Multidisciplinary Modeling & Simulation Multiconference

2724-0355 © 2023 The Authors.
doi: 10.46354/i3m.2023.foodops.003

Mixing of non-Newtonian fluids: from CFD simulations to predictive performance metrics

Natalya Lysova[1,*], Federico Solari[1], Claudio Suppini[1], Michele Bocelli[1], Andrea Volpi[1] and Roberto Montanari[1]

[1] Department of Engineering and Architecture, University of Parma, Parco Area delle Scienze 181/A, Parma (PR), 43124, Italy

*Corresponding author. Email address: natalya.lysova@unipr.it

Abstract

Mixing is widely adopted in the food industry to homogenize the chemical and physical properties of fluids, with a strong impact on the quality of the products. The complex rheological behaviour of most food fluids influences the flow field in the domain, so particular attention must be paid during the design of the process. Dimensionless numbers are generally adopted to characterize mixing impellers in terms of power consumption and flow rate elaborated. Other key performance indicators (KPIs), assessing the mixing quality, were defined in a previous study. These indicators are based on simulation data, so they cannot be calculated without carrying out dedicated simulations. In this study, a computational fluid dynamics (CFD) simulation campaign was performed reproducing the mixing of a non-Newtonian fluid with pitched blade turbine impellers under different operating conditions. The results were used to draw insights into the process and generate predictive models of the simulation-based KPIs as a function of the geometric and operating conditions. In this way, the study aims to promote the use of the proposed KPIs to get insights that could not be derived using standard approaches. Future research activities will target the generalization of these models to account for more process features.

Keywords: mixing; computational fluid dynamics; simulation; key performance indicators; non-newtonian fluids

1. Introduction

Mixing is one of the fundamental processes in the food industry, as it allows for achieving the required food structure and characteristics through, e.g., blending, homogenization, emulsification, or inter-dispersion of phases, typically by providing kinetic energy to the fluids by means of rotating impellers (Cullen, 2009). It is generally performed inside stirred vessels that, based on the process features, type of treated product, and the necessary production yield, may assume different configurations in terms of tank dimensions and geometry, impeller geometry, orientation and position of the impeller shaft inside the tank. Usually, the tanks are provided with baffles, which are static barriers aimed at disrupting the fluid flow to prevent the formation of swirling and vortexes, while enhancing turbulence and ensuring thorough mixing. Based on the fluid flow generated, impellers can be classified into radial, axial, and mixed.

To characterize an impeller, two dimensionless quantities are usually adopted: power and flow numbers. The power number (N_p) provides insights into the power requirements and consumption associated with the mixing process. This number can be leveraged to define efficient mixing systems, select the appropriate motor size, compare different impeller designs, and scale up mixing systems from laboratory

to industrial scale. The flow number (N_q), on the other hand, is linked to the mixing performance of the system, indicating how well the fluid is recirculated in the vessel thanks to the action of the impeller. Like N_p, N_q is essential for scale-up operations, process optimization, and comparison of alternative configurations.

As stated, mixing is widely used in the food industry. In this context, fluids are often complex, and they may contain dispersed particles or different phases. Overall, their rheological behaviour may strongly differ from conventional fluids where the shear rate is directly proportional to the force applied through a constant viscosity value. The fluids processed in the food industry often exhibit non-Newtonian rheological behaviour, meaning that they do not have a constant value of viscosity. Their rheological behaviour is therefore described through an apparent viscosity, that is generally dependent on the shear rate and the temperature; furthermore, these fluids often require a minimum yield stress to be imparted to the fluid in order to initiate flow. With regard to the mixing processes, the non-Newtonian rheological behaviour usually results in the formation of zones around the impeller characterized by higher velocity values and mixing degree, referred to as "caverns", and zones more distant from the impeller where the mixing is less efficient and the velocities significantly lower. Since this phenomenon strongly impacts the quality of the treatment and the final product, it must be accurately accounted for when designing a mixing process.

Non-Newtonian fluids have been described with several analytic models over time (Steffe, 1996). However, as the apparent viscosity may vary strongly in different points of the domain based on the local characteristics, it can be extremely difficult to accurately predict the flow behaviour and characterize the physical phenomena in applications of practical relevance in the food industry. To this end, computational fluid dynamics (CFD) is an essential tool that allows practitioners to accurately estimate the parameters of interest through numerical simulation, by solving the governing equations of interest in an appropriately discretized domain. CFD has been extensively applied to food industry processes in the last decades, proving its effectiveness and precision even in the case of complex fluids and multiphase flows (Ian Wilson and John Chew, 2023; Szpicer et al., 2023).

A selection of key performance indicators (KPIs) of mixing quality and efficiency have been introduced in (Ferretti et al., 2013). These include the following three indicators: the velocity index (*VI*) that evaluates the velocity field inside the vessel to prevent stagnation zones, the mixing homogeneity index (*MHI*) that measures the uniformity of the velocity inside the agitator, and the mixing effectiveness index (*MEI*) that is calculated to estimate the efficiency of a given mixing system in avoiding the stratification of product inside the tank. These coefficients can be calculated based on the velocity module and its components at each node of the discretized system, obtained through CFD simulation. A limitation of this approach is that to estimate these KPIs, CFD simulations must be carried out, requiring a certain degree of expertise in simulation, availability of appropriate software and hardware, and time.

In this study, a CFD simulation campaign was carried out reproducing the mixing of a non-Newtonian fluid by means of pitched blade turbine (PBT) impellers with a 45° pitch angle. Two different PBT geometries, with two and four blades, were evaluated in this preliminary phase. This choice was motivated by the fact that these impeller geometries are often adopted in practical industrial applications, and they have been extensively studied in the literature, so a lot of data is available to validate the simulation model and findings. The simulation campaign was carried out by reproducing different flow conditions, quantified in terms of dimensionless generalized Reynolds number. The results of the simulations were used to characterize the two impeller geometries, calculating for each operating condition the power and flow numbers, as well as the KPIs introduced in (Ferretti et al., 2013). Finally, a set of correlations was developed to express the CFD-derived KPIs in terms of the generalized Reynolds number and the number of impeller blades, to overcome the limitations of the previous study and generate predictive metrics for mixing efficiency.

2. State of the art

Mixing processes have been extensively evaluated in the literature over the years, with many fundamental works dating back to the early 1900s, investigating the flow characteristics and the power consumption of several impeller geometries. Researchers have addressed the mixing of both Newtonian and non-Newtonian fluids of industrial interest, deriving fundamental relationships between the system features and the operating conditions, able to characterize the performance of the systems and facilitate the scale-up operations. In this context, indices such as the dimensionless power and flow numbers (Rushton et al., 1950, Weetman and Oldshue, 1988), their trend under different flow conditions, characterization of the flow behaviour of agitations systems, definition of the relationship between rotational speed and the average shear rate in the domain were derived (Metzner and Otto 1957; Metzner et al., 1961). Based on these works, correlations have been developed to estimate the dimensionless mixing numbers based on the system features. A fundamental relationship has been derived in (Chapple et al., 2002) and it is commonly adopted to estimate the power number for four-blade PBT impellers (4 PBT). Validated correlations allow to estimate the performances of mixing systems without having to resort to, sometimes complex, experimental techniques. Techniques for measuring the system power consumption, necessary to derive the power

number include: measurement of the current drawn by the motor, measurement of the torque on the tank by using a bearing in combination with a spring scale, measurement of the temperature rise in the fluid and, the most direct and used technique, measurement of the torque on the shaft by means of torque transducers (Chapple et al., 2002). The techniques used to evaluate the flow field and the velocities in the system include laser doppler velocimetry (LDV) and particle image velocimetry (PIV) (Alonzo-Garcia et al., 2019).

In the last decades, the development of computational instrumentation and techniques such as CFD allowed researchers to leverage numerical simulation to reproduce agitated vessels with different geometric configurations under different operating conditions. After validating the model, it is indeed possible to carry out simulation campaigns and draw fundamental insight based on the knowledge of the distribution of the physical quantities of interest in, ideally, every point of the domain, with a degree of accuracy depending on the discretization performed. Several CFD techniques have been developed and adopted over time to simulate systems with both rotating and stationary components, such as the time-dependent sliding mesh model (SM), the steady-state approximation by means of multiple reference frame (MRF) and, a variation of the latter, the circumferential averaging model (CA) (Aubin et al., 2004).

As mixing causes the formation of vortices and turbulence in the system, the choice of the appropriate turbulence model is essential to guarantee the accuracy of the results. To this end, Reynolds-averaged Navier-Stokes (RANS) models, which allow to model the turbulence with an appropriate degree of accuracy for practical engineering applications, have been studied in the literature. Their performance has been extensively evaluated in combination with different techniques of generation of the computational grid that, obviously, greatly impacts the results of the simulation (Alonzo-Garcia et al., 2019; Coroneo et al., 2011; Aubin et al., 2004).

In the past years, CFD has been used to design, characterize and optimize several impeller geometries and agitation systems. It has been of great importance in understanding the flow field generated by impellers with complex geometries, non-Newtonian fluids, as well as systems with multiple impellers or rotor-stator combinations (Ameur, 2016; Ameur, 2015; John et al., 2022; Ferretti et al., 2013). In (Ferretti et al., 2013), new CFD-based KPIs have been introduced to evaluate the performance of mixing systems for non-Newtonian fluids containing dispersed particles. These KPIs, however, depend on the availability of data related to the flow field in a multitude of points inside the domain, leaving room for further investigation and generalization of these indicators.

3. Materials and Methods

The simulation model was set up to reproduce the conditions presented in (Alzonzo-Garcia et al., 2019). This study was selected because it performed both experimental and simulative evaluations of a pitched blade turbine with four blades (4 PBT) and a pitch angle θ=45°, comparing the results and the deviations from the expected values in the case of different discretization grids and turbulence models.

In particular, the simulated domain consisted of a tank with a 4 PBT, used to agitate water, and four baffles arranged along the wall of the tank. The main geometrical characteristics of the system included the diameter of the tank (T), the height of the liquid (H), the diameter of the impeller (D), the clearance off-bottom (C), the thickness (t) and projected high of the blades (h), the thickness (t_B) and the width(w_B) of the baffles. Starting from T=250 mm, most of the geometrical features of the system were defined based on commonly adopted ratios, in order to reproduce the conditions studied in the literature and obtain general, thus scalable, results, independent of the actual system measures. In particular, $D = T/3$, $C = T/3$ and $w_B = T/10$. The diameter of the impeller hub was defined based on a standard value of hub-to-tip diameter ratio Ψ for pitched blade turbines, which was assumed to be 0.25. The hub diameter was then calculated as $d_H = \Psi \cdot D$. The hub height was modelled to be slightly over h, by adding 1 mm above and below the projection of the blade. As the diameter of the shaft (d_S) was not mentioned in (Alonzo-Garcia et al., 2019), it was assumed to have the dimensions described in (Chapple et al., 2002) that analyzed a system with comparable measures. A second analysis was carried out by modifying the geometry of the domain. In particular, the number of blades (n_{BL}) was set equal to two (2 PBT). The geometrical features of the simulated domain are summarized in Table 1.

Table 1. Geometrical features of the simulated domain

Symbol	Description	Value	Units
T	diameter of the tank	250	mm
H	liquid height	250	mm
D	diameter of the impeller	83.33	mm
C	clearance off-bottom	83.33	mm
n_{BL}	number of impeller blades	4 (4 PBT) and 2 (2 PBT)	units
θ	blade pitch angle	45	°
t	blade thickness	1.5	mm
h	projected height of the blade	14.3	mm
t_B	baffle thickness	3.5	mm
w_B	baffle width	25	mm
d_H	hub diameter	15.9	mm
h_H	hub height	16.3	mm
d_S	shaft diameter	6.4	mm

The simulation campaign, therefore, was performed considering two PBT geometries with a different number of blades, used to agitate a non-Newtonian fluid under different flow conditions. The results of the simulations were used to calculate the power number N_p (eq. 1), (Rushton et al., 1950), and the flow number N_q (eq. 2). In these equations P is the shaft power, Q is the elaborated flow rate, ρ is the fluid density, N is the rotational velocity and D is the diameter of the impeller.

$$N_p = \frac{P}{\rho \cdot N^3 \cdot D^5} \quad (1)$$

$$N_q = \frac{Q}{N \cdot D^3} \quad (2)$$

The KPIs introduced in (Ferretti et al., 2013), evaluating the quality of the mixing process, were:

- *VI*: Velocity index defined as the fraction of volume with a velocity higher than a threshold value;
- *MEI*: Mixing efficacy index evaluating the ability to prevent stratification by comparing the entity of the vertical kinetic energy, due to the vertical velocity component v_y, against the total energy supplied to the fluid quantified based on the three velocity components v_x, v_y and v_z (eq.3);
- *MHI*: Mixing homogeneity index evaluating the ratio of the standard deviation of velocity in the tank to a maximum standard deviation value calculated by assuming that half of the domain has the maximum velocity value and the other half domain has a null velocity (eq. 4);
-

$$MEI = \frac{\sum_{i=1}^{n} v_{y,i}^2}{\sum_{i=1}^{n}\left(v_{x,i}^2 + v_{y,i}^2 + v_{z,i}^2\right)} \quad (3)$$

$$MHI = 1 - \frac{\sigma}{\sigma_{max}} \quad (4)$$

The simulation analysis targeted the mixing of a non-Newtonian fluid, a 0.1% mixture of Xanthan gum, with apparent viscosity η modelled according to the power law Ostwald-de Waele model (eq. 5).

$$\eta = K\dot{\gamma}^{n-1} \quad (5)$$

In the equation K is the consistency index, n is the flow behaviour index and $\dot{\gamma}$ is the shear rate. In particular, n represents the deviation of the rheological behaviour of a fluid from the Newtonian conditions, which are characterized by a direct proportionality between the applied shear stress and the resulting shear rate, leading to a constant viscosity value. Fluids are defined as "Newtonian" when n=1, and "non-Newtonian" otherwise (Steffe, 1996). As for the characterization of the fluid, the data derived from the measurements performed in (Venneker et al., 2010) were used: for the 0.1% Xanthan gum solution, K was $74.8 \cdot 10^{-3}$ Pa·s^n and n was 0.56 (Figure 1). Since $n < 1$, the fluid presents a shear-thinning (pseudoplastic) rheological behaviour: in this case, η is lower in the regions with higher shear rate values, i.e., near the impeller blades.

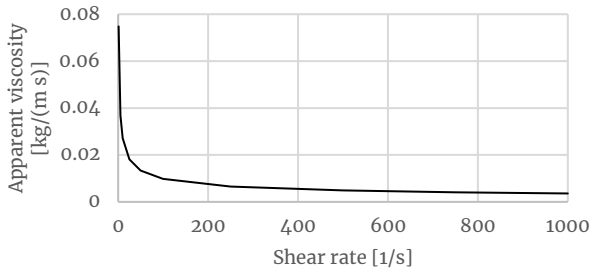

Figure 1. Apparent viscosity at different shear rate values

As stated, the simulation campaign was performed under different flow conditions. In particular, for each geometry, five different cases from laminar to fully turbulent conditions were evaluated. In the case of mixing applications, the flow conditions are usually classified according to the appropriately formulated dimensionless Reynolds number (eq. 6).

$$Re = \frac{\rho \cdot N \cdot D^2}{\mu} \quad (6)$$

In the equation ρ is the fluid density, μ is the viscosity and N is the impeller rotational speed. As the fluid is non-Newtonian and does not have a constant viscosity value, the generalized Reynolds number can be introduced, accounting for the rheological coefficients of the fluid at an average shear rate value $\dot{\gamma}_{ave}$. $\dot{\gamma}_{ave}$ can be estimated according to (Metzner and Otto, 1957) as the rotational speed N of the impeller multiplied by a constant k_s that is a weak function of the impeller type (eq.7). The values of k_s for different impellers in the case of Newtonian and non-Newtonian fluids were introduced in (Metzner et al., 1961), deriving an average value of 11.5 for flat blade impellers and tank-to-impeller ratios $T/D \geq 3$. The generalized Reynolds number, formulated for mixing applications in the case of shear-thinning fluids, therefore, can be expressed according to eq.8 (Ameur, 2016).

$$\dot{\gamma}_{ave} = k_s \cdot N \quad (7)$$

$$Re_g = \frac{\rho \cdot N^{2-n} \cdot D^2}{K \cdot {k_s}^{n-1}} \quad (8)$$

The different flow conditions were simulated by modifying the value of Re_g by acting on N (Table 2). The highest Re_g was defined to fall under fully turbulent conditions, that are generally recognized to occur at Re>20000. In this way, it was possible to validate the results of the simulations for the 4 PBT impeller with the correlation derived in (Chapple et al., 2002), usually adopted to calculate the reference fully turbulent power number ($N_{p,ft}$). For 4 PBT impellers operating with a standard configuration characterized by $D = T/3$ and $C = T/3$, the reference $N_{p,ft}$ is assumed equal to 1.27. The results for the flow number were compared with the reference value of N_q=0.79 derived by Weetman and Oldshue (1988).

Table 2. Flow conditions, in terms of generalized Reynolds number, evaluated during the simulation campaign

Case	N [rpm]	Re_g
1	2	23
2	7	142
3	35	1443
4	85	5177
5	260	25898

3.1. Simulation campaign

To perform the CFD simulations it was necessary to create the geometric model of the system, generate the mesh by dividing the volume into a finite number of elements and, finally, set up the simulation by defining the appropriate models and boundary conditions for the problem. The 3D geometry of the device was reproduced with ANSYS SpaceClaim for the two cases of PBT with 2 and 4 blades (Figure 2). As the CFD simulations targeted the motion of the fluid, the final 3D model consisted of the volume of fluid constrained by the tank walls and around the impeller. Neither the walls nor the impeller geometries were modelled, as they were not significant for the present analysis.

The domain was then discretized with ANSYS Meshing with a tetrahedral mesh, reproducing the sizing settings defined in (Alonzo-Garcia et al., 2019) after a mesh sensitivity analysis. In particular, the sizing of the elements on the impeller was set equal to 0.375 mm. Other sizing settings included the element size of 2.75 mm and program-controlled inflation at the impeller walls to accurately solve for the velocity gradients. The final mesh, consisting of $3.3 \cdot 10^6$ elements as the one adopted in (Alonzo-Garcia et al., 2019), was then transferred to ANSYS Fluent for the calculation activities (Figure 3). The mesh of the system with the 2 PBT impeller was generated analogously, resulting in $3 \cdot 10^6$ elements.

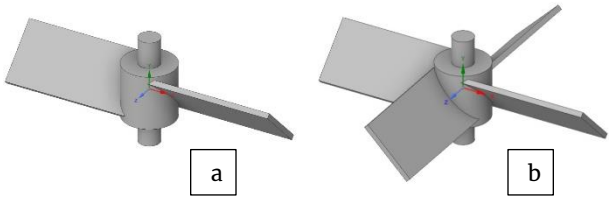

Figure 2. Geometries of impeller evaluated: (a) 2 PBT and (b) 4 PBT

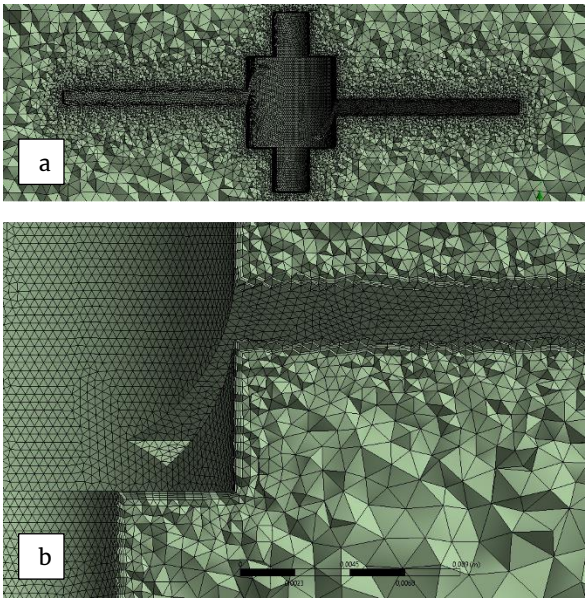

Figure 3. Mesh with an increased number of elements around the impeller (a) and detail of the inflation layers (b).

As the mixing process was fully periodic, the simulations were performed under steady-state conditions. To account for the movement of the fluid due to the rotation of the impeller, the multiple reference frame (MRF) model was adopted. To this end, moving and stationary zones must be defined; then, according to the MRF approach, the equations of interest can be solved in the stationary and moving zones independently, considering the interaction between them at the interface. In the present case, the moving zone consisted of a cylindric volume surrounding the impeller, with a height equal to 2.6·h and a diameter of 1.4·D; the stationary zone consisted of the remaining fluid domain around the mobile zone (Figure 4). The "Frame motion" condition was enabled for the moving domain, and the appropriate impeller rotational velocity was assigned to it for each simulated case. The impeller walls were then defined as moving walls, with motion conditions derived from the adjacent moving cell zone.

A first simulation with water and a rotation velocity of 500 rpm was performed to validate the torque experimentally measured by (Alonzo-Garcia et al., 2019). Then, the simulation campaign with 2 PBT and 4 PBT impeller geometries was performed under different flow conditions as summarized in Table 2.

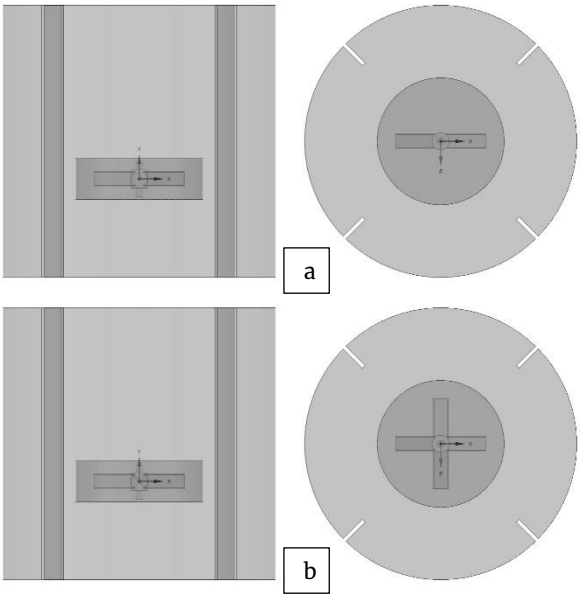

Figure 4. 3D geometry of the simulated fluid domain, with the division into moving and stationary zones:(a) 2 PBT and (b) 4 PBT

In particular, cases 1, 2 and 3 were simulated under laminar conditions, while for cases 4 and 5 the modelling of the turbulence was included. According to the results obtained by (Alonzo-Garcia et al., 2019), $k-\omega$ *SST* turbulence model (Menter, 1994) was selected. With regards to the solution methods, the SIMPLE algorithm was used for the pressure-velocity coupling, the second-order scheme was used for the pressure interpolation, and the second-order upwind was used for the turbulent kinetic energy k and the specific dissipation rate ω. To evaluate the solution, the convergence criterion was set at 10^{-5} for the residuals of all solved equations, and the values of torque on the impeller and velocity in a given point were monitored until they assumed a constant value. After performing the first simulation with tetrahedral mesh, a second one was carried out after converting the mesh to polyhedra, thus decreasing the number of elements and, at the same time, increasing the quality of the mesh. The results of the two simulations were then compared to verify whether this conversion had an impact on the obtained values. After verifying the correspondence of the results, the simulation campaign was carried out with the polyhedral mesh, decreasing the computation time required.

3.2. Calculation of mixing numbers and KPIs

The power required for the mixing, P, was derived from the torque T calculated on the impeller walls as reported in eq. 9 and it was then used to calculate N_p (eq. 1). Conversely, N_q was calculated based on the vertical flow rate directed towards the bottom, passing through a circular plane slightly larger than the impeller (D_{plane}=0.043 m) and located 3 mm below the blades according to eq. 2 (Figure 5). This value was computed in ANSYS CFD-Post with a personalized expression (eq. 10) used to calculate the average value of v_y on the plane. According to CFD-Post notation, the symbol @ indicates the location at which the expression is calculated.

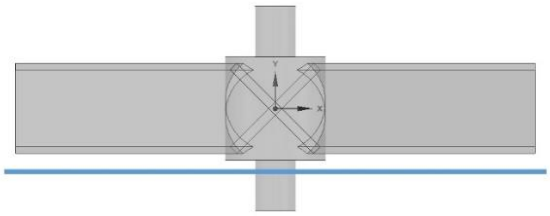

Figure 5. Details of the plane defined for the flow rate evaluation

$$P = 2\pi \cdot N \cdot T \tag{9}$$

$$v_{y,ave} = areaAve\left(if\ v_y < 0\ [m\ s^{-1}], v_y, 0\ [m\ s^{-1}]\right)@Plane \tag{10}$$

The CFD-derived values of the velocity module and its v_x, v_y and v_z components in each node of the simulated domain were then used to calculate the mixing KPIs *VI*, *MEI* and *MHI* introduced in (Ferretti et al., 2013). Most of the elaborations were performed in CFD-Post using personalized expressions. To perform these calculations, an auxiliary volume (*Vol*) was generated to include both the moving and the stationary zones.

To calculate *VI*, an evaluation of the velocity in every node was performed, by assessing whether the value was higher than the volume-weighted average in the domain $\bar{v}$, $\bar{v}$+standard deviation (σ), $\bar{v}+2\sigma$ and $\bar{v}+3\sigma$. In particular, the number of cells where this comparison was *True* was determined (VI_{num}). VI_{num} was then divided by the number of elements (*Num*) to calculate *VI* (eq. 11, eq. 12).

$$VI_{num} = CountTrue(Velocity > volumeAve(Velocity)@Vol)@Vol \tag{11}$$

$$VI = \frac{VI_{num}}{Num} \tag{12}$$

To calculate *MEI*, two expressions were defined, one to calculate the sum of squares of v_y (MEI_y) and one to calculate the sum of the sum of squares of v_x, v_y, and v_z (MEI_{xyz}) at every node (eq. 13, eq. 14). *MEI* was then calculated at the ratio of the two (eq.15).

$$MEI_y = sum(v_y{}^2)@Vol \quad (13)$$

$$MEI_{xyz} = sum(v_x{}^2 + v_y{}^2 + v_z{}^2)@Vol \quad (14)$$

$$MEI = \frac{MEI_y}{MEI_{xyz}} \quad (15)$$

To calculate *MHI* it was necessary to calculate the standard deviation in the domain σ and the reference σ_{max}. The numerator (Dev) of the variance of velocity in the domain was calculated with a personalized expression in CFD-Post, and the standard deviation σ was then derived (eq. 16, eq. 17). The maximum standard deviation has been calculated as defined in eq. 18, by assuming half domain with null velocity, half domain with maximum velocity v_{max}, and an average velocity v_{ave} equal to $v_{max}/2$. *MHI* was finally calculated as defined in eq. 3.

$$Dev = sum((Velocity - volumeAve(Velocity)@Vol)^2) \quad (16)$$

$$\sigma = \sqrt{\frac{Dev}{Num}} \quad (17)$$

$$\sigma_{max} = \sqrt{\frac{Num/2 * (0 - v_{ave})^2 + Num/2 * (v_{max} - v_{ave})^2}{Num}} \quad (18)$$

DesignExpert statistical software was used to evaluate the significance of Re_g and n_{BL} to the KPIs through analysis of variance (ANOVA). Finally, numerical correlations were developed to be able to estimate the indicators based on the system and fluid characteristics without the need to perform dedicated CFD simulations. In particular, n_{BL} accounts for the impeller blade configuration, while Re_g effectively summarizes the operating conditions in terms of rotational velocity, impeller diameter, fluid density and rheological behaviour.

4. Results and Discussion

After performing the simulations, the results were analyzed in terms of velocity contours on a longitudinal section plane, to have an overview of the flow field inside the domain (Figure 6). It can be observed how the flow becomes more directed towards the bottom of the tank as the rotational velocity increases, while it tends to expand mostly in a radial direction at lower *N* values. Another observation can be made about the cavern, i.e., the well-mixed region, which appears to be wider with a 4 PBT impeller. This occurs because of the better mixing obtainable at the same rotational velocity with two additional impeller blades. Also, the rheological behaviour of the fluid plays an important part, as it tends to present lower apparent viscosity values in proximity to the blades. In Figure 6 it can also be observed how the velocity values below the impeller tend to be higher in the case of a 4 PBT impeller. This is confirmed by the mean velocity value inside the domain, $\bar{v}$, reported in Table 3 and Table 4 for 2 PBT and 4 PBT impellers, respectively.

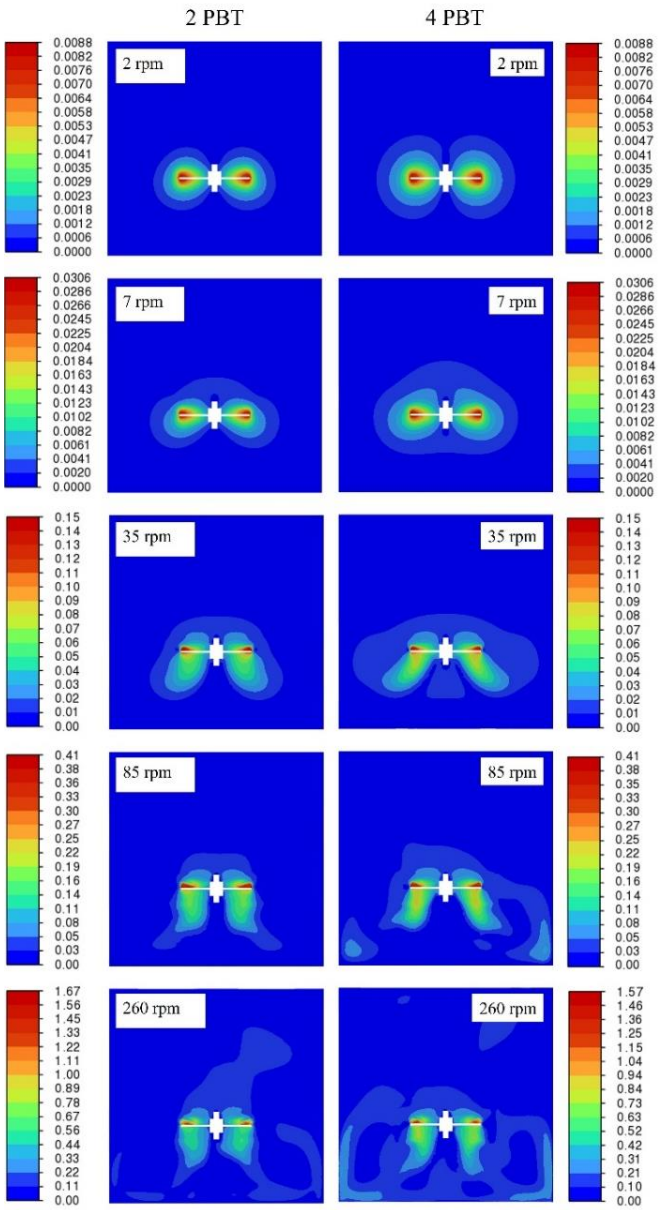

Figure 6. Contours of velocity on a longitudinal section plane for 2 PBT and 4 PBT impellers at different rotational velocities.

Table 3. Results of the simulations with the 2 PBT impeller

N [rpm]	2	7	35	85	260
Torque [N m]	0.000006	0.000022	0.000170	0.000986	0.009206
N_p	9.145	2.560	0.782	0.769	0.768
v_y on Plane	0.00031	0.00116	0.02897	0.07844	0.25756
N_q	0.094	0.100	0.499	0.556	0.597
$\bar{v}$	0.00021	0.00069	0.00492	0.02090	0.09835
VI (v> $\bar{v}$)	14.85%	14.87%	15.13%	15.15%	14.70%
VI (v> $\bar{v}+\sigma$)	8.98%	10.23%	9.73%	8.23%	7.95%
VI (v> $\overline{v+2\sigma}$)	6.18%	6.09%	5.72%	5.67%	5.26%
VI (v> $\bar{v}+3\sigma$)	4.33%	4.22%	3.93%	3.78%	3.39%
MEI	0.33%	0.64%	5.36%	11.10%	18.02%
MHI	65.65%	66.61%	71.29%	73.58%	79.47%

Table 4. Results of the simulations with the 4 PBT impeller

N [rpm]	2	7	35	85	260
Torque [N m]	0.000011	0.000036	0.000302	0.001512	0.015333
N_p	15.203	4.199	1.389	1.180	1.279
v_y on Plane	0.00033	0.00114	0.03210	0.09263	0.29842
N_q	0.099	0.098	0.552	0.656	0.691
$\bar{v}$	0.00030	0.00105	0.00638	0.02290	0.10572
VI (v> $\bar{v}$)	18.02%	18.09%	18.39%	18.69%	17.92%
VI (v> $\bar{v}+\sigma$)	12.29%	12.21%	11.61%	11.35%	10.84%
VI (v> $\overline{v+2\sigma}$)	8.35%	8.21%	7.63%	7.43%	6.96%
VI (v> $\bar{v}+3\sigma$)	4.77%	4.67%	4.37%	4.15%	3.87%
MEI	0.20%	0.45%	5.40%	9.87%	19.05%
MHI	57.41%	58.55%	64.44%	68.10%	67.21%

Indeed, $\bar{v}$ obtained with the 4 PBT is higher at every N value compared to the other impeller geometry.

The other simulation results reported in Table 3 and Table 4 include the torque value on the impeller used to calculate N_p, the vertical velocity component directed towards the bottom of the tank, used to calculate N_q, as well as the dimensionless numbers and the KPIs introduced in (Ferretti et al., 2013). The obtained N_p and N_q numbers are plotted against Re_g in Figure 7. In accordance with the results from the literature, N_p behaves as a negative exponential in the laminar region, while it tends to be constant at higher Re_g. It can be observed that, because of the higher blade count, N_p is higher in the case of the 4 PBT impeller. N_q on the other hand, tends to rapidly increase in the laminar region as Re_g increases, and then tends to a constant value in the turbulent region. Also in this case N_q is higher for the 4 PBT impeller, suggesting that the flow rate pumped towards the bottom of the tank increases with two additional blades.

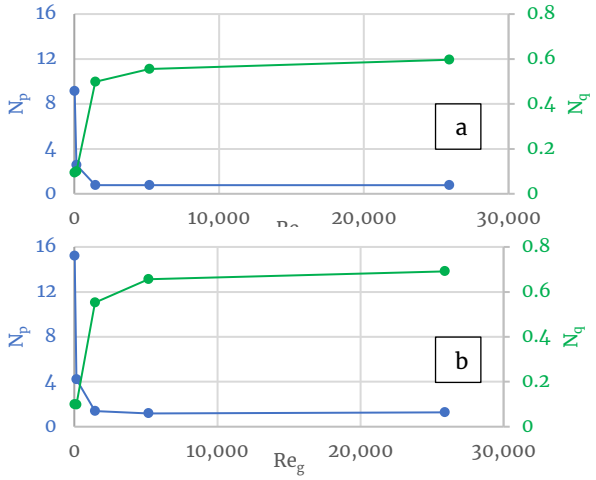

Figure 7. Power and flow number in function of Re_g for (a) 2 PBT impeller and (b) 4 PBT impeller

The calculated mixing KPIs are plotted against Re_g in Figures 8-10. In particular, *VI* indicators represented in Figure 8 assess the portion of the domain with a velocity value higher than $\bar{v}$, $\bar{v}+\sigma$, $\bar{v}+2\sigma$ and $\bar{v}+3\sigma$. It results that the indicator that compares the velocity values with the average, $VI(\bar{v})$, tends to present a constant value regardless of the flow regime, while those that account for higher velocity values, i.e., $VI(\bar{v}+\sigma)$, $VI(\bar{v}+2\sigma)$ and $VI(\bar{v}+3\sigma)$, consistently decrease as Re_g increases.

MEI, which accounts for the vertical fraction of kinetic energy in the system as an indicator of mixing efficiency, appears to be independent of n_{BL}, in the configuration considered and with this specific fluid, but it varies strongly with Re_g (Figure 9). This trend replicates the results presented in the velocity contour plots (Figure 6), where a much more significant v_y component can be observed at higher N, and therefore Re_g, values.

MHI, which compares the standard deviation of velocity in the system against a reference value, on the other hand, varies with both n_{BL} and Re_g. In particular, it increases in the laminar region, and then it remains constant under turbulent flow conditions (Figure 10). The *MHI* calculated for the 2 PBT impeller appears to be higher than the KPI calculated for 4 PBT. This can be traced back to the particular configuration simulated: as there is only one impeller used to agitate a viscous fluid in a relatively large tank, most of the volume is characterized by a very low velocity value, thus $\bar{v}$ tends to be low. As the velocity in the 2 PBT configuration has been observed to be generally lower, its deviation from $\bar{v}$ is overall smaller.

The calculated mixing KPIs allow to gain valuable insights about the the mixing process and its efficiency under different operating conditions, but to calculate them it is necessary to have access to a large amount of data in several points of the domain, obtainable by performing CFD simulations of the process.

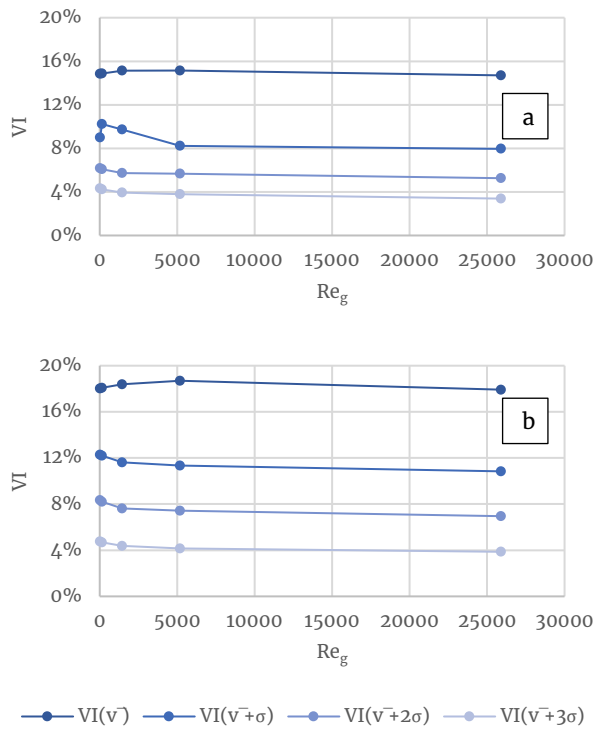

Figure 8. *VI* KPI for (a) 2 PBT impeller and (b) 4 PBT impeller

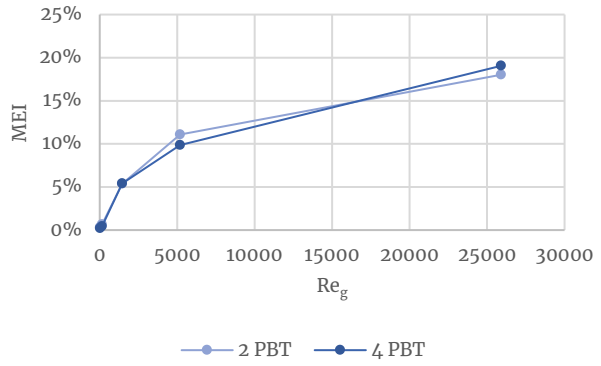

Figure 9. MEI mixing KPI

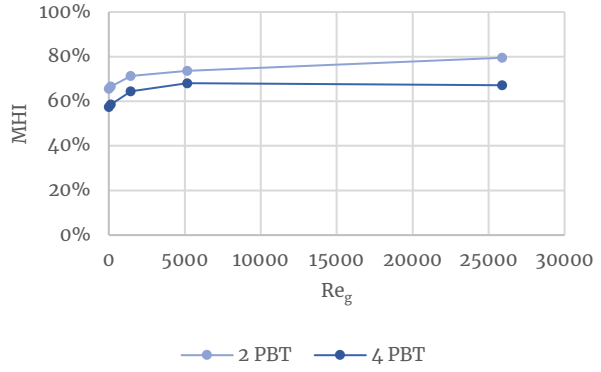

Figure 10. MHI mixing KPI

This approach, however, requires high computational power and is time-consuming. To this end, the input data in terms of Re_g and n_{BL}, and the results in terms of *VI*, *MEI* and *MHI*, were imported into DesignExpert to evaluate the significance of Re_g and n_{BL} and generate predictive models of the KPIs. Based on the software suggestions, the linear model was used for all KPIs.

With regard to $VI(\bar{v})$, as expected, only n_{BL} was significant. The generated model, with R^2=0.98, is reported in eq. 19. On the other hand, $VI(\bar{v}+\sigma)$, $VI(\bar{v}+2\sigma)$ and $VI(\bar{v}+3\sigma)$ turned out to be significantly impacted by both Re_g and n_{BL}. It can be inferred that the portion of the fluid with $v > \bar{v}$ depends mostly on the impeller geometry, while the incidence of the regions with higher velocity values is impacted also by the type of fluid and the flow regime. The models for $VI(\bar{v}+2\sigma)$ and $VI(\bar{v}+3\sigma)$ are reported in eq. 20 and eq. 21 (R^2=0.95 and 0.83). As observed in Figure 9, *MEI* was impacted only by Re_g. This behaviour was confirmed by ANOVA, and the model generated, with R^2=0.85, is reported in eq. 22. *MHI*, on the other hand, is significantly impacted by both Re_g and n_{BL}, and can be estimated by eq. 23 (R^2=0.76).

$$VI(\bar{v}) = 0.117 + 0.0164 \cdot n_{BL} \tag{19}$$

$$VI(\bar{v}+2\sigma) = 0.0409 - 3.64 \cdot 10^{-7} \cdot Re_g + 0.00965 \cdot n_{BL} \tag{20}$$

$$VI(\bar{v}+2\sigma) = 0.0369 - 2.96 \cdot 10^{-7} \cdot Re_g + 0.00217 \cdot n_{BL} \tag{21}$$

$$MEI = 0.0284 + 6.42 \cdot 10^{-6} \cdot Re_g \tag{22}$$

$$MHI = 0.771 + 3.64 \cdot 10^{-6} \cdot Re_g - 0.0409 \cdot n_{BL} \tag{23}$$

5. Conclusions

Mixing is one of the essential operations in food processing and it can greatly influence the quality of the final product. As most food fluids present a complex rheological behaviour, that can strongly impact the flow field in the domain, it can be difficult to calculate the performance of a mixing process with analytic methods. To this end, CFD can be leveraged to derive simulation-based KPIs that were introduced in (Ferretti et al., 2013) to assess the flow field inside the domain, the mixing efficiency and homogeneity.

The aim of this study was to evaluate the impact of the input operating conditions, in terms of the number

of impeller blades and the generalized Reynolds number, on these KPIs and develop simple models for their estimation without the need to perform dedicated simulations. To this end, a simulation campaign was carried out, and the results were analyzed and fitted with linear models by means of statistical software. It was observed that in some cases both inputs were significant, while in others only one of them significantly impacted the indicator.

The generated models can be already used to preventively estimate the KPIs of the simulated mixing systems under different flow conditions within the considered range. Future research activities are required to build on this preliminary work and further generalize this modelling approach, developing predictive models of the mixing performances based on other fundamental parameters. To this end, a dedicated simulation campaign, defined according to DOE methodology, would be required to include in the analysis factors such as the tank diameter, the clearance off-bottom, the distance from the free surface, multiple impellers, and other fluids with different rheological behaviour, even containing dispersed particulate. In addition, experimental tests would be required to validate the results.

References

Alonzo-Garcia, A., Mendoza-Escamilla, V. X., Martinez-Delgadillo, S. A., Gonzalez-Neria, I., Gutiérrez-Torres, C. del C., & Jiménez-Bernal, J. A. (2019). On the performance of different RANS based models to describe the turbulent flow in an agitated vessel using non-structured grids and PIV validation. Brazilian Journal of Chemical Engineering, 36(1), 361–382. https://doi.org/10.1590/0104-6632.20190361s20180091

Ameur, H. (2015). Energy efficiency of different impellers in stirred tank reactors. Energy, 93, 1980–1988. https://doi.org/10.1016/j.energy.2015.10.084

Ameur, H. (2016). Mixing of complex fluids with flat and pitched bladed impellers: Effect of blade attack angle and shear-thinning behaviour. Food and Bioproducts Processing, 99, 71–77. https://doi.org/10.1016/j.fbp.2016.04.004

Aubin J, Fletcher DF, Xuereb C (2004) Modeling turbulent flow in stirred tanks with CFD: the influence of the modeling approach, turbulence model and numerical scheme. Exp Therm Fluid Sci 28:431–445

Chapple, D., Kresta, S. M., Wall, A., & Afacan, A. (2002). The Effect of Impeller and Tank Geometry on Power Number for a Pitched Blade Turbine. Chemical Engineering Research and Design, 80(4), 364–372. https://doi.org/10.1205/026387602317446407

Coroneo, M., Montante, G., Paglianti, A., & Magelli, F. (2011). CFD prediction of fluid flow and mixing in stirred tanks: Numerical issues about the RANS simulations. Computers&Chemical Engineering, 35(10),1959–1968. https://doi.org/10.1016/j.compchemeng.2010.12.007

Cullen, P. J. (Ed.). (2009). Food mixing: Principles and applications. John Wiley & Sons.

Ferretti, G., Montanari, R., Solari, F., & Vignali, G. (2013). Advanced Design of Industrial Mixers for Fluid Foods Using Computational Fluid Dynamics. International Journal of Food Engineering, 9(3), 309–325. https://doi.org/10.1515/ijfe-2013-0035

John, T. P., Fonte, C. P., Kowalski, A., & Rodgers, T. L. (2022). The effect of axial impeller geometry on the link between power and flow numbers. AIChE Journal, 69(3). Portico. https://doi.org/10.1002/aic.17871

Ian Wilson, D., & John Chew, Y. M. (2023). Fluid mechanics in food engineering. Current Opinion in Food Science, 51, 101038. https://doi.org/10.1016/j.cofs.2023.101038

Menter, F. R. (1994). Two-equation eddy-viscosity turbulence models for engineering applications. AIAA journal, 32(8), 1598-1605.

Metzner, A. B., Feehs, R. H., Ramos, H. L., Otto, R. E., & Tuthill, J. D. (1961). Agitation of viscous Newtonian and non-Newtonian fluids. AIChE Journal, 7(1), 3–9. https://doi.org/10.1002/aic.690070103

Metzner, A. B., & Otto, R. E. (1957). Agitation of non-Newtonian fluids. AIChE Journal, 3(1), 3–10. https://doi.org/10.1002/aic.690030103

Rushton, J.H., Costich, E.W. and Everett, H.J. (1950) Power Characteristics of Mixing Impellers. Chemical Engineering Progress, 46, 467-476.

Steffe, J. F. (1996). Rheological methods in food process engineering. Freeman press.

Szpicer, A., Bińkowska, W., Wojtasik-Kalinowska, I., Salih, S. M., & Półtorak, A. (2023). Application of computational fluid dynamics simulations in food industry. European Food Research and Technology, 249(6), 1411–1430. https://doi.org/10.1007/s00217-023-04231-y

Venneker, B. C. H., Derksen, J. J., & Van den Akker, H. E. A. (2010). Turbulent flow of shear-thinning liquids in stirred tanks—The effects of Reynolds number and flow index. Chemical Engineering Research and Design, 88(7), 827–843. https://doi.org/10.1016/j.cherd.2010.01.002

Weetman, R.J., Oldshue, J.Y., Power Flow and Shear Characteristics of Mixing Impellers. Proceedings of the 6th European Conference on Mixing. Pavia, Italy, 24–26 May, 1988.